EUROPEAN ORGANIZATION FOR PARTICLE PHYSICS

OPAL-PN-153
September 13, 1994

A Test of $\mathcal{CP}$-Invariance in $Z^0 \longrightarrow \tau^+\tau^-$ Using Optimal Observables

The OPAL Collaboration

Abstract

Using 27 490 $Z^0 \rightarrow \tau^+\tau^-$ decays, accumulated in 1991, 1992 and 1993 with the OPAL detector at LEP, a direct test of $\mathcal{CP}$-invariance in the neutral current reaction $e^+e^- \longrightarrow \tau^+\tau^-$ is performed by measuring $\mathcal{CP}$-odd observables which are proportional to the weak dipole moment of the τ-lepton. A new method based on optimal $\mathcal{CP}$-odd observables constructed from the τ flight and spin directions is employed. More sensitive measurements of the real and - for the first time - the imaginary part of the weak dipole moment with highest possible signal to noise ratio are obtained. No evidence for a non-zero expectation value of the considered observables and hence for $\mathcal{CP}$-violation is observed. An upper limit on the weak dipole moment of $|\,\mathrm{Re}(d_\tau^w)\,| < 7.9 \times 10^{-18}\ e \cdot \mathrm{cm}$ and $|\,\mathrm{Im}(d_\tau^w)\,| < 4.5 \times 10^{-17}\ e \cdot \mathrm{cm}$ with 95% confidence level is obtained.

1 Introduction

In the Standard Model, $\mathcal{CP}$-violation has its origin in the charged current couplings among quarks and is described by a phase in the CKM-matrix [1]. Violation of $\mathcal{CP}$-symmetry has so far not been observed in neutral current reactions, and the Standard Model does not predict any measurable effects there [2].

In neutral current processes $\mathcal{CP}$-violation can be introduced if the participating particles possess electric or weak dipole moments. For two reasons it is advantageous to use the $\mathrm{Z}^0 \to \tau^+\tau^-$ decay for the search of $\mathcal{CP}$-violation. First, the $\mathcal{CP}$-violating dipole moment is related to the spin of the outgoing fermion. Due to its short lifetime the τ-lepton decays inside the detector and indirectly transfers information about its spin to the energies and momenta of its decay products. Second, $\mathcal{CP}$-violating models exist [2] in which the magnitude of the lepton dipole moment depends on the mass of the fermion to the third power, thus favoring processes with heavy fermions.

$\mathcal{CP}$-violation in $\mathrm{Z}^0 \to \tau^+\tau^-$ decays can be studied by measuring $\mathcal{CP}$-odd observables. If $\mathcal{CP}$-invariance holds, the mean value of these observables must be zero. Any observation of a non-zero expectation value of $\mathcal{CP}$-odd observables would indicate physics beyond the Standard Model.

Taking into account operators with mass dimension $d \leq 6$, the $\mathcal{CP}$-violating effective Lagrangian of the $\tau^+\tau^-$ production vertex is given by [2]

$$\mathcal{L}_{CP} \;=\; -\frac{i}{2}\bar{\tau}\sigma^{\mu\nu}\gamma_5\tau\,\left(\,d_\tau^e(q^2)F_{\mu\nu} \;+\; d_\tau^w(q^2)Z_{\mu\nu}\,\right) \tag{1}$$

where $F_{\mu\nu}$ and $Z_{\mu\nu}$ are the electromagnetic and weak field tensors. The electric and weak dipole form factors are denoted by $d_\tau^e(q^2)$ and $d_\tau^w(q^2)$, respectively. They determine the strength of the $\mathcal{CP}$-violating amplitude and may have a real as well as an imaginary part. At LEP the momentum transfer q is given by $q^2 = m_{\mathrm{Z}}^2$; $d_\tau^w(m_{\mathrm{Z}}^2)$, which dominates at this q^2, is now called the weak dipole moment. The $\mathcal{CP}$-violating transition amplitude $T_{\mathcal{CP}}$, with coupling strength d_τ^w, occurs in addition to the Standard Model amplitude T_{SM}. For large d_τ^w the interaction $\mathcal{L}_{\mathcal{CP}}$ gives rise to a non-negligible $\mathcal{CP}$-even contribution, $|T_{\mathcal{CP}}|^2$, to the cross section $\mathrm{d}\sigma \propto |T_{\mathrm{SM}} + T_{\mathcal{CP}}|^2$ and the partial width $\Gamma(\mathrm{Z}^0 \to \tau^+\tau^-)$. In principle a measurement of the partial width for $\mathrm{Z}^0 \to \tau^+\tau^-$ does not constitute a test of $\mathcal{CP}$-invariance. However, it can be used to determine d_τ^w under the assumption that no interaction outside the Standard Model other than $\mathcal{L}_{\mathcal{CP}}$ contributes to the width. With this method an upper limit on d_τ^w from $\Gamma(\mathrm{Z}^0 \to \tau^+\tau^-)$ was derived in [15][16]. The $\mathcal{CP}$-odd interference term, in contrast, gives rise to $\mathcal{CP}$-violating effects.

2 $\mathcal{CP}$-odd Observables

$\mathcal{CP}$-odd observables $\mathcal{O}$ have various transformation properties under time reversal. $\mathcal{CP}$-odd and $\mathcal{T}$-odd observables $\mathcal{O}^{\mathcal{T}^-}$ transform $\mathcal{CPT}$-even. Their mean values are proportional to $\mathrm{Re}(d_\tau^w)$. $\mathcal{CP}$-odd and $\mathcal{T}$-even observables $\mathcal{O}^{\mathcal{T}^+}$ transform $\mathcal{CPT}$-odd. Given $\mathcal{CPT}$-invariance, which is assumed throughout this paper, a non-zero mean value would be proportional to

$\mathrm{Im}(d_\tau^w)$. This requires absorptive parts in a $\mathcal{CP}$-non-conserving interaction.

Let us consider the reaction

$$e^+e^- \longrightarrow \tau^+(k_+)\,\tau^-(k_-) \longrightarrow A^+(p_A)\,B^-(p_B)\,\nu_\tau\bar{\nu}_\tau \tag{2}$$

where A and B are hadronic or leptonic final states emerging from τ^+ and τ^- decays, respectively. In the presence of a weak dipole moment the following relations hold:

$$\begin{aligned} \langle \mathcal{O}^{\mathcal{T}^-} \rangle_{AB} &= \frac{m_Z}{e} c_{AB}\,\mathrm{Re}(d_\tau^w) \\ \langle \mathcal{O}^{\mathcal{T}^+} \rangle_{AB} &= \frac{m_Z}{e} f_{AB}\,\mathrm{Im}(d_\tau^w)\ , \end{aligned} \tag{3}$$

i.e., the mean values of the observables $\mathcal{O}^{\mathcal{T}^\pm}$ are directly proportional to the weak dipole moment. The dimensionless proportionality constants c_{AB} and f_{AB} are called *sensitivities* and depend on the respective τ decay modes A, B. (See Section 5.) Many observables can be constructed which transform odd under $\mathcal{CP}$, such as $T_{ij} = (\mathbf{p}_A - \mathbf{p_B})_i(\mathbf{p}_A \times \mathbf{p}_B)_j$, which was used in previous analyses [15][16]. The optimal choice is obviously the one which maximizes the 'signal-to-noise' ratio

$$R^\pm = \sqrt{\frac{\langle \mathcal{O}^{\mathcal{T}^\pm} \rangle^2}{\langle (\mathcal{O}^{\mathcal{T}^\pm})^2 \rangle - \langle \mathcal{O}^{\mathcal{T}^\pm} \rangle^2}} \quad . \tag{4}$$

This condition is met by observables of the form [3]

$$\mathcal{O}^{\mathcal{T}^\pm} = \frac{\mathrm{d}\sigma_{\mathcal{CP}}^{\mathcal{T}^\pm}}{\mathrm{d}\sigma_{\mathrm{SM}}}\ . \tag{5}$$

Here $\mathrm{d}\sigma_{\mathcal{CP}}^{\mathcal{T}^\pm}$ are the terms in the differential cross section for $e^+e^- \to \tau^+\tau^-$ which are $\mathcal{CP}$-odd and $\mathcal{T}$-odd ($\mathcal{T}^-$) or $\mathcal{CP}$-odd and $\mathcal{T}$-even ($\mathcal{T}^+$), respectively, and $\mathrm{d}\sigma_{\mathrm{SM}}$ is the differential cross section of the Standard Model. Using the 'shorthand notation' $\mathrm{d}\sigma = \mathrm{d}\sigma_0 M_{\mathrm{SM}} + \mathrm{d}\sigma_1 M_{\mathcal{CP}}^{\mathrm{Re}} + \mathrm{d}\sigma_2 M_{\mathcal{CP}}^{\mathrm{Im}} + ...$, and neglecting all terms of the τ pair spin density matrix [4], which are proportional to the small neutral vector coupling constants g_V ($g_V/g_A = 0.074 \pm 0.006$ [5]), the leading terms of the differential cross sections in (5) are given by

$$\mathrm{d}\sigma_{\mathcal{CP}}^{\mathcal{T}^+} \propto M_{CP}^{\mathrm{Re}} = (\hat{\mathbf{k}}\,\hat{\mathbf{q}}_e)\left(\hat{\mathbf{k}} \times (\mathbf{S}^+ - \mathbf{S}^-)\right)\hat{\mathbf{q}}_e \tag{6}$$

$$\mathrm{d}\sigma_{\mathcal{CP}}^{\mathcal{T}^-} \propto M_{CP}^{\mathrm{Im}} = (\hat{\mathbf{k}}\,\hat{\mathbf{q}}_e)\left[(\hat{\mathbf{k}}\,\mathbf{S}^+)(\hat{\mathbf{q}}_e\mathbf{S}^-) - (\hat{\mathbf{k}}\,\mathbf{S}^-)(\hat{\mathbf{q}}_e\mathbf{S}^+)\right] \tag{7}$$

$$\begin{aligned} \mathrm{d}\sigma_{\mathrm{SM}} \propto M_{SM} = 1 &+ (\hat{\mathbf{k}}\,\hat{\mathbf{q}}_e)^2 + \mathbf{S}^+\mathbf{S}^-(1 - (\hat{\mathbf{k}}\,\hat{\mathbf{q}}_e)^2) - 2(\hat{\mathbf{q}}_e\mathbf{S}^+)(\hat{\mathbf{q}}_e\mathbf{S}^-) \\ &+ 2(\hat{\mathbf{k}}\,\hat{\mathbf{q}}_e)\left[(\hat{\mathbf{k}}\,\mathbf{S}^+)(\hat{\mathbf{q}}_e\mathbf{S}^-) + (\hat{\mathbf{k}}\,\mathbf{S}^-)(\hat{\mathbf{q}}_e\mathbf{S}^+)\right]. \end{aligned} \tag{8}$$

Here $\hat{\mathbf{q}}_e$ is the direction of the electron beam, $\hat{\mathbf{k}}$ is the flight direction of the positive τ and the $\mathbf{S}^\pm$ are the spin vectors of the $\tau^\pm$ leptons in their respective rest systems. The observable used in this analysis then becomes

$$\tilde{\mathcal{O}}^{\mathcal{T}^\pm} = \frac{M_{\mathcal{CP}}^{\mathrm{Re/Im}}}{M_{\mathrm{SM}}}\ . \tag{9}$$

Neither the τ spin nor the τ flight direction can be measured directly. However, in reaction (2) the τ momentum $\hat{\mathbf{k}}$ can be reconstructed up to a twofold ambiguity assuming two-body kinematics and assuming that the Z^0 rest frame corresponds to the laboratory frame which means that initial state radiation is neglected. The ambiguity can be resolved in principle by means of the information obtained from a precise vertex detector measuring the track positions close to the interaction point in three dimensions as proposed in [6]. This would increase our sensitivity to $\mathcal{CP}$-violation by approximately 10%. Up to the year 1992 OPAL's Si microvertex detector provided only track measurements in $r-\phi$, so that the ambiguity could only be resolved with a probability of about 65% using $\tau \to \pi\nu$ decays. It was therefore not considered any further in this analysis. We currently reconstruct only the component of the τ^+ momentum in the decay plane of the final state particles. It is given by

$$\mathbf{k} \;=\; u\hat{\mathbf{p}}_A \;+\; v\hat{\mathbf{p}}_B \tag{10}$$

$$u \;=\; \frac{\alpha_A \;+\; \hat{\mathbf{p}}_A\hat{\mathbf{p}}_B\alpha_B}{1 \;-\; (\hat{\mathbf{p}}_A\hat{\mathbf{p}}_B)^2} \quad , \qquad v \;=\; -\frac{\alpha_B \;+\; \hat{\mathbf{p}}_A\hat{\mathbf{p}}_B\alpha_A}{1 \;-\; (\hat{\mathbf{p}}_A\hat{\mathbf{p}}_B)^2} \quad , \tag{11}$$

where hats denote unit momenta in the laboratory frame, and

$$\alpha_i \;=\; \frac{\sqrt{s} \;-\; m_\tau^2 \;-\; m_i^2}{2|\mathbf{p}_i|} \qquad (i \;=\; A,\; B)\;, \tag{12}$$

where $\sqrt{s}$ is the c.m. energy.

As pointed out in [7][8], the differential partial width for any decay of a polarized τ is $\mathrm{d}\Gamma \;=\; |\bar{M}|^2/2m_\tau \cdot (1 + \mathbf{S}\,\mathbf{h})\, dLips$, where $|\bar{M}|^2$ is the squared matrix element and $\mathbf{S}$ is the three-dimensional polarization vector in the τ rest frame. If the τ momentum $\mathbf{k}$ is known, the 'polarimeter vector' $\mathbf{h}$ can be computed from the momentum of the daughter particles in the laboratory frame [9]. modes into $e\,\nu\bar{\nu}$, $\mu\,\nu\bar{\nu}$, $\pi\,\nu$, $\pi\pi^0\,\nu$, $3\pi\,\nu$ are selected exclusively. The condition of maximum emission probability means that we use for the spin orientation the direction of the polarimeter vector, which leads us to the expressions [3]:

$$[\mathbf{S}^\pm]_{\tau\to\ell\nu_\ell\nu} \;=\; -m_\tau \frac{\pm\,(2(k^\pm p_{\ell\pm} - m_\ell^2)(h - g^\pm) + \frac{1}{2}g^\pm(f^\pm + m_\tau^2 - m_\ell^2))\cdot\mathbf{k} - f^\pm\mathbf{p}_{\ell\pm}}{(k^\pm p_{\ell\pm})\,(3m_\tau^2 + 3m_\ell^2 - 4k^\pm p_{\ell\pm}) \;-\; 2m_\tau m_\ell}$$

$$\text{where} \qquad f^\pm = m_\tau^2 + 3m_\ell^2 - 4k^\pm p_{\ell\pm}\;, \quad g^\pm = \frac{E_{\ell\pm}}{m_\tau} - \frac{k^\pm p_{\ell\pm}}{m_\tau(k^0 + m_\tau)}$$

$$h = \frac{E_{\ell\pm}}{m_\tau} - 1 - \frac{(k^0)^2 - m_\tau^2}{m_\tau(k^0 + m_\tau)}$$

$$[\mathbf{S}^\pm]_{\tau\to\pi\nu} \;=\; \frac{2}{m_\tau^2 \;-\; m_\pi^2}\left(\mp m_\tau\,\mathbf{p}_{\pi\pm} \;+\; \frac{m_\tau^2 \;+\; m_\pi^2 \;+\; 2m_\tau E_{\pi\pm}}{2(k_0 \;+\; m_\tau)}\mathbf{k}\right)$$

$$[\mathbf{S}^\pm]_{\tau\to\rho\nu\to\pi\pi^0\nu} \;=\; \mp\,\frac{\mp H_0^\pm\mathbf{k} \;+\; m_\tau\mathbf{H}^\pm \;+\; \mathbf{k}\cdot(\mathbf{k}\mathbf{H}^\pm)/(k_0 \;+\; m_\tau)}{(k_\pm H_\pm) \;-\; m_\tau^2\cdot(p_{\pi\pm} \;-\; p_{\pi^0})^2}$$

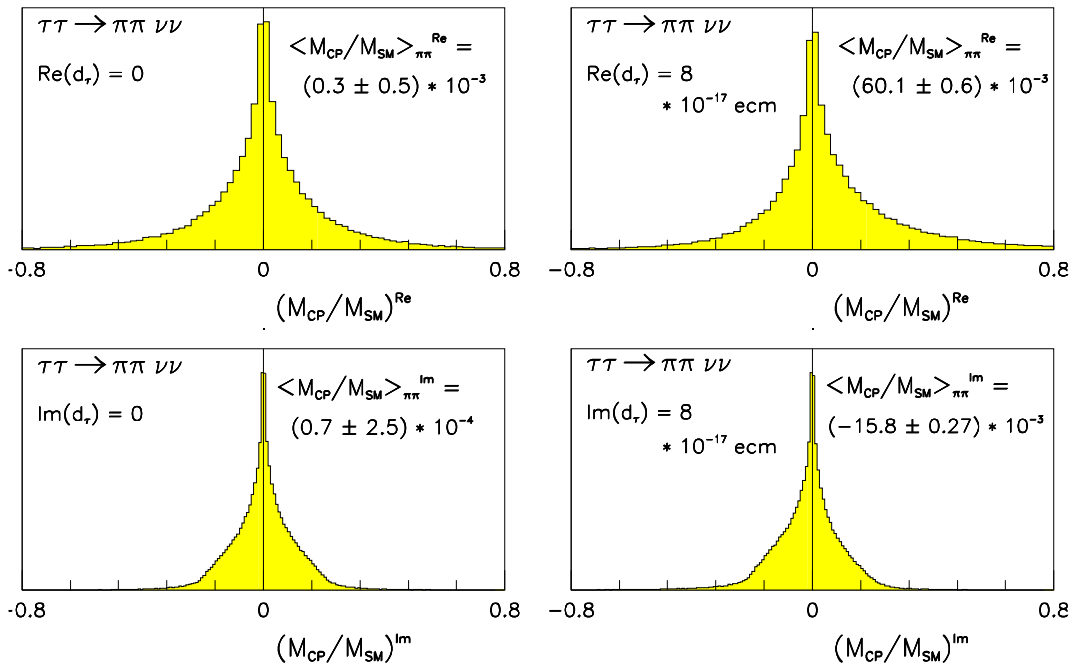

Figure 1: $M_{\mathcal{CP}}/M_{\rm SM}$ in the $\tau^+\tau^- \to \pi^+\pi^-\nu\bar{\nu}$ decay for zero d_τ^w (left side) and $\mathrm{Re}(d_\tau^w)$=$\mathrm{Im}(d_\tau^w) = 8\times10^{-17}\,e$·cm (right side).

and

$$(H^\pm)^\nu \;=\; 2(p_{\pi^\pm} - p_{\pi^0})^\nu (p_{\pi^\pm} - p_{\pi^0})^\mu (k_\pm)_\mu + (p_{\pi^\pm} + p_{\pi^0})^\nu (p_{\pi^\pm} - p_{\pi^0})^2$$

The expression for the 3π decay channel follows the notation

$$\tau^\pm(k) \;\longrightarrow (a_1\nu \to \rho\pi\nu) \longrightarrow\; \pi^\pm(p^\pm)\,\pi^0(p_1)\,\pi^0(p_2)\;,$$

which is equivalent to a decay into three charged pions by rotation of isospin assuming isospin invariance[1]. One obtains

$$[\mathbf{S}^\pm]_{\tau\to a_1\nu\to\rho\pi\nu\to3\pi\nu} \;=\; \mp m_\tau\,(\mathbf{Z}^\pm/N^\pm) \tag{13}$$

where

$$\mathbf{Z}^\pm \;=\; \Big[\,\Big(|F_\rho^1|^2(kh_1) + \mathrm{Re}F_\rho^1F_\rho^2(kh_2)\Big)\,\boldsymbol{\xi}_1 + \Big(|F_\rho^2|^2(kh_2) + \mathrm{Re}F_\rho^1F_\rho^2(kh_1)\Big)\,\boldsymbol{\xi}_2 - \frac{1}{2}(h_1h_2)\mathrm{Re}(F_\rho^1+F_\rho^2)^2\boldsymbol{\eta} + \mathrm{Im}F_\rho^1F_\rho^2\,\boldsymbol{\zeta}\,\Big]^\pm$$

$$N^\pm \;=\; \Big[\,\mathrm{Re}\Big(F_\rho^1(kh_1)+F_\rho^2(kh_2)\Big)^2 - \frac{1}{2}k(k-Q)(h_1h_2)\mathrm{Re}(F_\rho^1+F_\rho^2)^2 + \mathrm{Im}F_\rho^1F_\rho^2(kH)\,\Big]^\pm$$

defining

[1] In this case the denotation follows $\tau^\pm \to \pi^\mp(p^\mp)\,\pi^\pm(p_1)\,\pi^\pm(p_2)$.

$$\boldsymbol{\xi}^{\pm}_{1/2} \;=\; \mathbf{Y}^{\pm}(h^{\pm}_{1/2})\;, \quad \boldsymbol{\eta}^{\pm} \;=\; \mathbf{Y}^{\pm}(k^{\pm}-Q^{\pm})\;, \quad \boldsymbol{\zeta}^{\pm} \;=\; \mathbf{Y}^{\pm}(H^{\pm})\;,$$

where

$$\mathbf{Y}^{\pm} \;=\; \mathbf{Y}^{\pm}(b) \;=\; \pm\frac{b^0}{m_\tau}\mathbf{k} \;-\; \mathbf{b} \;-\; \frac{\mathbf{kb}}{m_\tau(E_\tau+m_\tau)}\mathbf{k}\;, \qquad b=b\,(b^0,\mathbf{b})\;.$$

The four-vector $H^{\pm}$ arises from permutation terms in the $\tau \to 3\pi$ decay matrix and is given by

$$H^{\pm} \;=\; \left(\begin{array}{l} (k-Q)_2\lambda_{13} \;+\; (k-Q)_1\lambda_{32} \;+\; (k-Q)_3\lambda_{21} \\ (k-Q)_3\lambda_{02} \;+\; (k-Q)_0\lambda_{23} \;+\; (k-Q)_2\lambda_{30} \\ (k-Q)_0\lambda_{31} \;+\; (k-Q)_3\lambda_{10} \;+\; (k-Q)_1\lambda_{03} \\ (k-Q)_1\lambda_{20} \;+\; (k-Q)_2\lambda_{01} \;+\; (k-Q)_0\lambda_{12} \end{array}\right)^{\pm}$$

where

$$\lambda^{\pm}_{\mu\nu} \;=\; (h^1_\mu h^2_\nu \;-\; h^1_\nu h^2_\mu)^{\pm}$$

and

$$h^{\pm}_{1/2} \;=\; \left[\, p - p_{1/2} - Q\frac{Q(p-p_{1/2})}{(Q)^2} \,\right]^{\pm}\;, \qquad Q^{\pm} \;=\; p^{\pm}+p_1+p_2\;.$$

$F^{1/2}_{\rho^{\pm}} \;=\; F_\rho\left((p^{\pm}+p_{1/2})^2\right)$ is the Breit-Wigner propagator describing the ρ resonance

$$F_\rho(u) \;=\; \frac{m^2_\rho}{m^2_\rho - u - i\sqrt{u}\Gamma(u)}$$

with the momentum dependent, p-wave corrected width

$$\Gamma(u) \;=\; \Gamma_\rho\,\frac{m^2_\rho}{(m^2_\rho-4m^2_\pi)^{3/2}}\,\frac{(u-4m^2_\pi)^{3/2}}{u}\;.$$

In these expressions the vector $\mathbf{k}$ describes the real τ flight direction, but in the following measurement it is replaced by the approximation (10).

Figure 1 shows the distributions of such $\mathcal{CP}$-odd observables (9) generated by Monte Carlo simulation. For non-zero dipole moments the expectation values of the respective observables are no longer zero.

3 τ-Pair Selection

This analysis uses τ decay modes with one and three charged tracks. The data were recorded at LEP during 1991, 1992 and 1993. The integrated luminosity represents 69.1 pb^{-1} distributed in energy around the Z^0 peak and corresponds to 88 600 produced $\tau^+\tau^-$ events.

The topology of $e^+e^- \to \tau^+\tau^-$ events is characterized by a pair of back-to-back, narrow jets with low particle multiplicity. These characteristics are exploited by dividing the event into jets whose tracks and clusters are assigned to cones of half-angle 35°. For the selection of τ-pairs we follow our standard selection criteria.

Three main background sources have to be considered. $Z^0 \to q\bar{q}$ events are removed by requiring between one and six tracks which passed standard quality cuts and not more than ten clusters in the electromagnetic calorimeter. Background from two photon events is removed by cuts on the visible energy. In addition the minimal total transverse momentum has to be 2 GeV when the visible energy is below 18 GeV. We also require an angle of acollinearity smaller than 15° between the jet axes. A less important type of background arises from cosmic rays. This is suppressed by time-of-flight-requirements and by the location of the event vertex and the event topology. Details can be found in [10].

The remaining events are almost entirely lepton pairs; $e^+e^- \to e^+e^-$ and $e^+e^- \to \mu^+\mu^-$ events are removed by cuts on the energy deposited in the electromagnetic calorimeter, the momenta and/or signals in the muon chambers.

In the data of the years 1991-1993 71147 τ-pairs have been found. This corresponds to an efficiency of about 80%.

4 Selection of τ Decay Channels

To select the one-prong τ decay channels and the three-prong modes a maximum likelihood method is employed, combining different informations measured for an individual event. The measured values of several variables are compared to properly normalized reference distributions taken from Monte Carlo calculations for all decay channels under consideration. An event is assigned to the particular decay channel for which it has the maximum likeli-

Monte Carlo τ-decay channel	reconstruction efficiency (%) barrel				overlap				endcaps			
1 prong	e	μ	π	ρ	e	μ	π	ρ	e	μ	π	ρ
e	94.7	0.0	0.9	2.4	95.7	0.0	0.5	0.4	90.5	0.0	0.6	1.5
μ	0.0	97.0	1.8	0.7	0.0	92.8	5.2	1.4	0.0	90.1	8.8	0.4
π	0.4	3.8	79.2	10.5	0.4	4.8	60.8	20.2	1.5	6.8	68.2	15.3
ρ	0.1	0.0	7.4	57.5	0.9	0.5	6.3	42.3	1.4	0.7	8.9	37.4
$a_1 \to \pi\ 2\pi^0$	0.0	0.0	0.5	10.3	0.3	0	0.3	11.0	0.3	0.0	1.8	11.3
3 prong	$a_1 \to 3\pi$		$3\pi\pi^0$		$a_1 \to 3\pi$		$3\pi\pi^0$		$a_1 \to 3\pi$		$3\pi\pi^0$	
$a_1 \to 3\pi$	65.1		15.4		69.1		13.3		59.4		10.9	
$a_1 \to 3\pi\pi^0$	24.3		48.1		22.5		56.9		27.8		38.6	

Table 1: Efficiencies and mixing probabilities for various τ decay channels after employing a maximum likelihood selection of exclusive one-prong and three-prong decays. The detector has been subdivided into three different geometrical regions named barrel, overlap, and endcaps.

decay channel $\tau \to \nu_\tau +$	purity (%) barrel	overlap	endcaps
$e\ \bar{\nu}_e$	$99.6 \pm 0.2 \pm 0.0$	$97.9 \pm 1.2 \pm 3.2$	$95.6 \pm 1.1 \pm 1.3$
$\mu\ \bar{\nu}_\mu$	$96.9 \pm 0.4 \pm 2.2$	$96.1 \pm 1.3 \pm 3.2$	$94.1 \pm 1.1 \pm 5.3$
$\pi\ (K)$	$78.4 \pm 1.2 \pm 7.0$	$73.2 \pm 3.7 \pm 7.5$	$63.4 \pm 2.2 \pm 7.1$
$\rho\ (K^*)$	$80.3 \pm 0.9 \pm 1.7$	$67.8 \pm 3.2 \pm 0.1$	$69.5 \pm 2.2 \pm 2.0$
$a_1 \to 3\pi_{3\,\mathrm{prong}}$	$77.5 \pm 1.6 \pm 5.0$	$73.6 \pm 4.8 \pm 5.0$	$80.3 \pm 3.0 \pm 5.0$

Table 2: Purity of the maximum likelihood selection. The errors are due to Monte Carlo statistics (first number) and systematics (second number).

hood. A detailed description of the τ decay channels considered and the variables used is given in the appendix. Assuming N_{var} variables and N_{par} decay channels, each variable i for τ decay channel j is distributed according to the (normalized) probability density function $f_i^j(x_i)$ given by a reference distribution taken from the Monte Carlo simulation [11][12] (KORALZ 38[13]/TAUOLA 1.5[14]). The probability for a particular configuration then is

$$p_i^j(x_i) \;=\; \frac{f_i^j(x_i)}{\sum_{j=1}^{N_{\mathrm{par}}} f_i^j(x_i)}\ . \tag{14}$$

The $p_i^j(x_i)$ are multiplied and normalized to obtain the likelihood function

$$\mathcal{L}^j(x) \;=\; \frac{\prod_{i=1}^{N_{\mathrm{var}}} p_i^j(x_i)}{\sum_{j=1}^{N_{\mathrm{par}}} \left(\prod_{i=1}^{N_{\mathrm{var}}} p_i^j(x_i) \right)}\ . \tag{15}$$

In Tables 1 and 2 the efficiencies and the purities of the maximum likelihood selection for the respective τ decay modes are listed. They are calculated in three different geometrical regions: barrel ($|\cos\theta| < 0.68$), overlap ($0.68 < |\cos\theta| < 0.76$), and endcap ($0.76 < |\cos\theta| < 0.95$), where θ is the polar angle between track and beam axis. The entries in table 1 are the probabilities for classifying the original decay channels in the left column as the final states given in the header lines. One notes that around 35% (barrel) of the ρ events are not identified as one of the considered τ decay products. The missing events are mostly detected in the $a_1^{1\ \mathrm{prong}}$ channel.

It is important to study the uncertainties of the background in the various τ decay channels because they dominate the systematic errors of the sensitivities (See Section 5). These uncertainties are derived by smearing the Monte Carlo reference distributions within ranges extracted from test samples in the data. The test samples of the variables from each detector component are obtained by excluding this detector component from the selection. Two independent likelihood selections were performed using information from

1. the μ-chambers, hadronic calorimeter, presampler, and $\mathrm{d}E/\mathrm{d}x$ data from the jet chamber.

2. the electromagnetic calorimeter only.

type of selection	puritiy (%) barrel				overlap				endcaps			
(see text)	e	μ	π	ρ	e	μ	π	ρ	e	μ	π	ρ
1.	96.2	95.8	51.2	51.6	93.3	94.3	47.3	50.9	85.5	92.6	39.8	56.7
2.	96.9	87.1	66.3	74.3	86.2	84.6	59.7	67.3	83.3	86.6	49.4	65.3

Table 3: Purities of the independent test samples.

Note that these selections of course have smaller efficiencies and purities than those in which all variables are used. The purities of the latter test samples can be found in Table 3.

In Figure 2 some examples of the comparison between data and Monte Carlo simulation are shown. The numbers on the top of each plot indicate the type of test sample used. The Monte Carlo distributions of most variables, for example XELS[2], AMRO, and NM7L compare quite well with the data. However, the electron peak in EOVP looks narrower in the Monte Carlo distribution[3] , which indicates that the momentum resolution is overestimated here. Additionally the μ peak in RSTL is too large in the Monte Carlo distribution[3]. To quantify the systematic uncertainties due to these disagreements between the Monte Carlo simulation and the data, we smeared the Monte Carlo reference distributions. The differences in the purities of the selected τ decay channels between the smeared and the non-smeared reference distributions are taken as the systematic uncertainties (Table 2). The effects of this process are largely dominated by the smearing of EOVP, which degrades the electron efficiency up to 11 %. Generally, the systematic uncertainties can be estimated quite conservatively, because the final measurement of d_τ^w is statistics dominated.

After all 27 490 events have been selected from the 1991, 1992 and 1993 data samples for the measurement of $\mathrm{Re}(d_\tau^w)$ and 12 834 for $\mathrm{Im}(d_\tau^w)$. Fewer events are used for the measurement of $\mathrm{Im}(d_\tau^w)$ because fewer τ decay modes are used. (See Table 4.)

5 The Sensitivities

The sensitivities c_{AB} and f_{AB} in (3) are the proportionality constants between the expectation values of the $\mathcal{CP}$-odd observables and the weak dipole moment. Table 4 shows that the hadronic decay channels which are the most powerful spin analyzers in the measurement of the τ-polarization also have the highest sensitivities. The sensitivities can be computed as weighted averages of the the $\mathcal{CP}$ observables $\mathcal{O}$ for each decay channel over the appropriate phase space with the differential cross section as weight factor. In this phase space integration, the particle momenta are restricted by the geometrical acceptance of the OPAL detector and the minimal energies are set to the energy cuts used in the data analysis. The sensitivities are functions of $\cos(\theta)$. Generally they have a maximum absolute value in the overlap region and are lower in the endcaps. The sensitivities of table 4 do not include the influence of detector resolution, background effects or radiative corrections.

[2]This and the following variables are defined and briefly explained in the appendix.

[3]of the year 1992 compared to the 1992 data

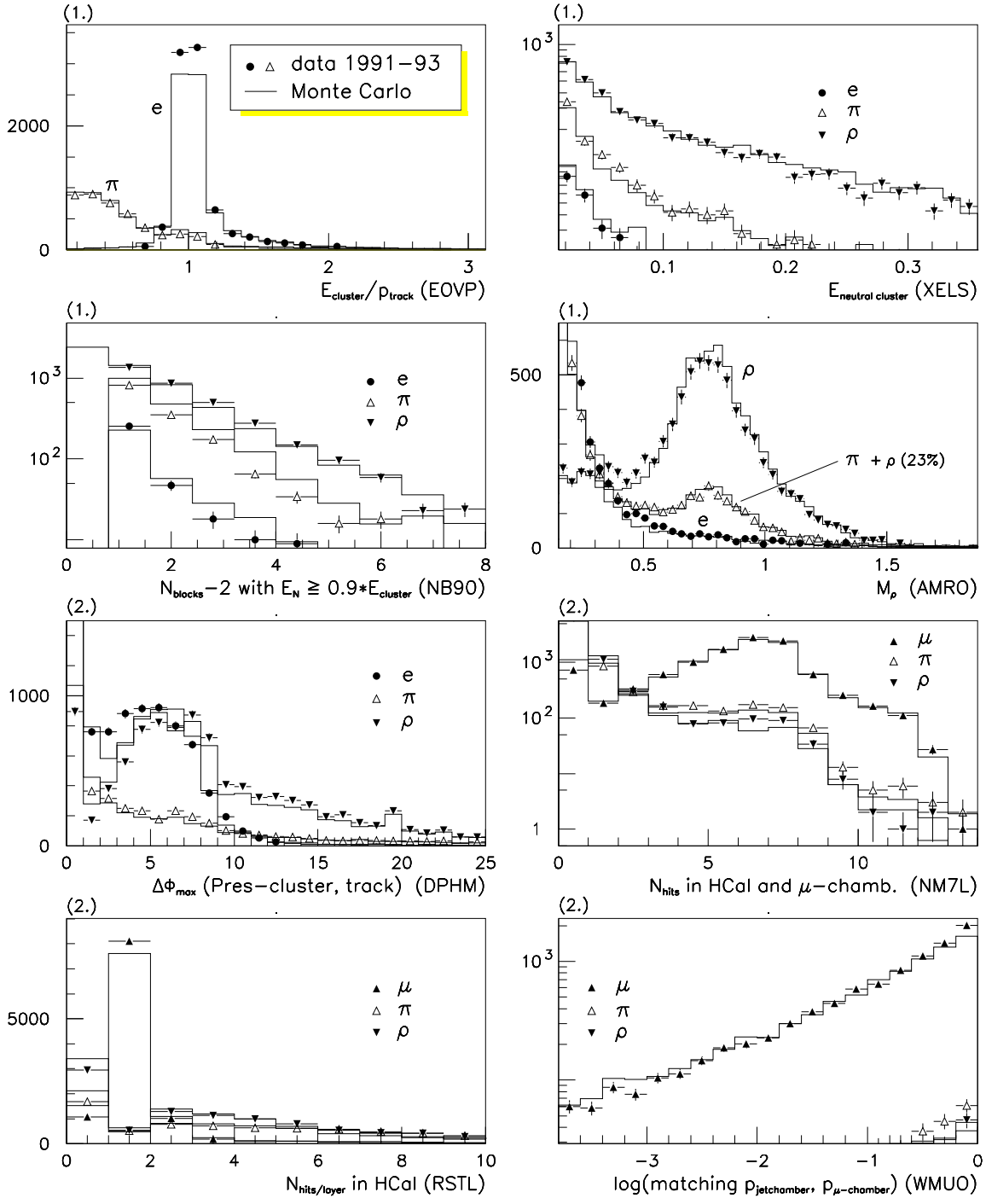

Figure 2: Comparison between data and Monte Carlo simulation using variables of independent test samples of type 1 and 2.

Systematic errors of and corrections to the sensitivities of the various τ decay channels arise from other τ decays as well as from non-τ background and from the experimental resolutions of the detector. The influence of radiative corrections, in particular initial state radiation, on

observable	decay channel $\tau^+\tau^- \to$	c_{AB}	f_{AB}
$\mathcal{O}_{\ell\ell}$	$\ell\ell\,\nu_\tau\bar{\nu}_\tau\nu_\ell\bar{\nu}_\ell$	-0.056 ± 0.002	-0.0046 $\pm$ 0.0006
$\mathcal{O}_{\ell\pi}$	$\ell\bar{\pi}\,\nu_\tau\bar{\nu}_\tau\nu_\ell$	0.048 ± 0.002	-
$\mathcal{O}_{\ell\rho}$	$\ell\bar{\rho}\,\nu_\tau\bar{\nu}_\tau\nu_\ell$	0.044 ± 0.002	-
$\mathcal{O}_{\ell 3\pi}$	$\ell 3\bar{\pi}\,\nu_\tau\bar{\nu}_\tau\nu_\ell$	0.041 ± 0.004	-
$\mathcal{O}_{\pi\pi}$	$\pi^+\pi^-\,\nu_\tau\bar{\nu}_\tau$	0.201 ± 0.003	-0.0450 $\pm$ 0.0050
$\mathcal{O}_{\pi\rho}$	$\pi\bar{\rho}\,\nu_\tau\bar{\nu}_\tau$	0.204 ± 0.004	-0.0265 $\pm$ 0.0050
$\mathcal{O}_{\pi 3\pi}$	$\pi 3\bar{\pi}\,\nu_\tau\bar{\nu}_\tau$	0.188 ± 0.008	-
$\mathcal{O}_{\rho\rho}$	$\rho\bar{\rho}\,\nu_\tau\bar{\nu}_\tau$	0.211 ± 0.005	-0.0490 $\pm$ 0.0050
$\mathcal{O}_{\rho 3\pi}$	$\rho 3\bar{\pi}\,\nu_\tau\bar{\nu}_\tau$	0.195 ± 0.008	-

Table 4: Sensitivities of various τ decay channels on the real part (c_{AB}) and the imaginary part (f_{AB}, some decays only) of the weak dipole moment before detector cuts.

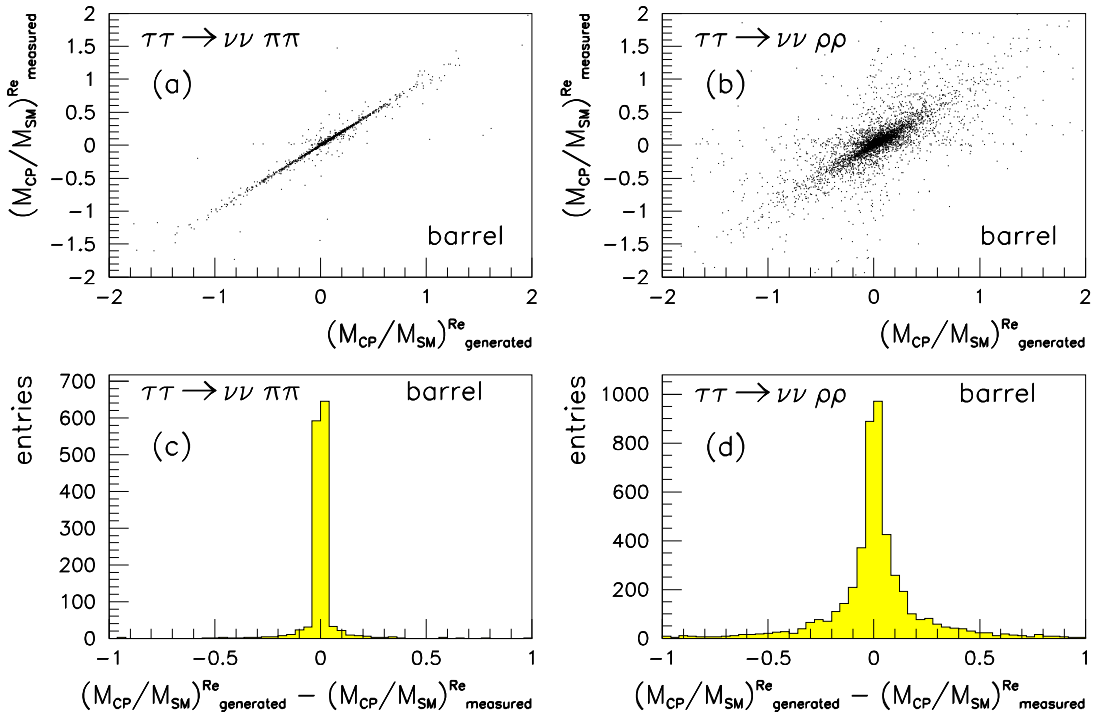

Figure 3: Correlations between generated and measured observables for $\tau^+\tau^- \to \pi^+\pi^-\,\nu\bar{\nu}$ and $\tau^+\tau^- \to \rho^+\rho^-\,\nu\bar{\nu}$ decays (a), (b). The mean values of the difference distributions (c), (d) determine the loss of sensitivity caused by the energy and momentum resolution of the detector.

the sensitivities is within the bounds of the numerical errors on the sensitivities (about 5%) and is thus neglected. In order to quantify the effects of the finite energy and momentum resolution on the sensitivities, we compare the $\mathcal{CP}$ observables obtained from generated and reconstructed momenta (see Figure 3), the latter taken from the detector simulation package GOPAL without any $\mathcal{CP}$-violation in the $Z^0 \to \tau^+\tau^-$ production. It was therefore additionally

introduced by weighting the observables with reference distributions generated by a $\mathcal{CP}$-violating Monte Carlo simulation (TAUMC[3]). The largest reduction (up to 15%) is observed for the sensitivities of decay channels including one or more π^0s in the final state, e.g. $\tau \to \rho\nu \to \pi\pi^0\nu$. The τ decay modes without neutral hadrons are reduced by less than 5%. The

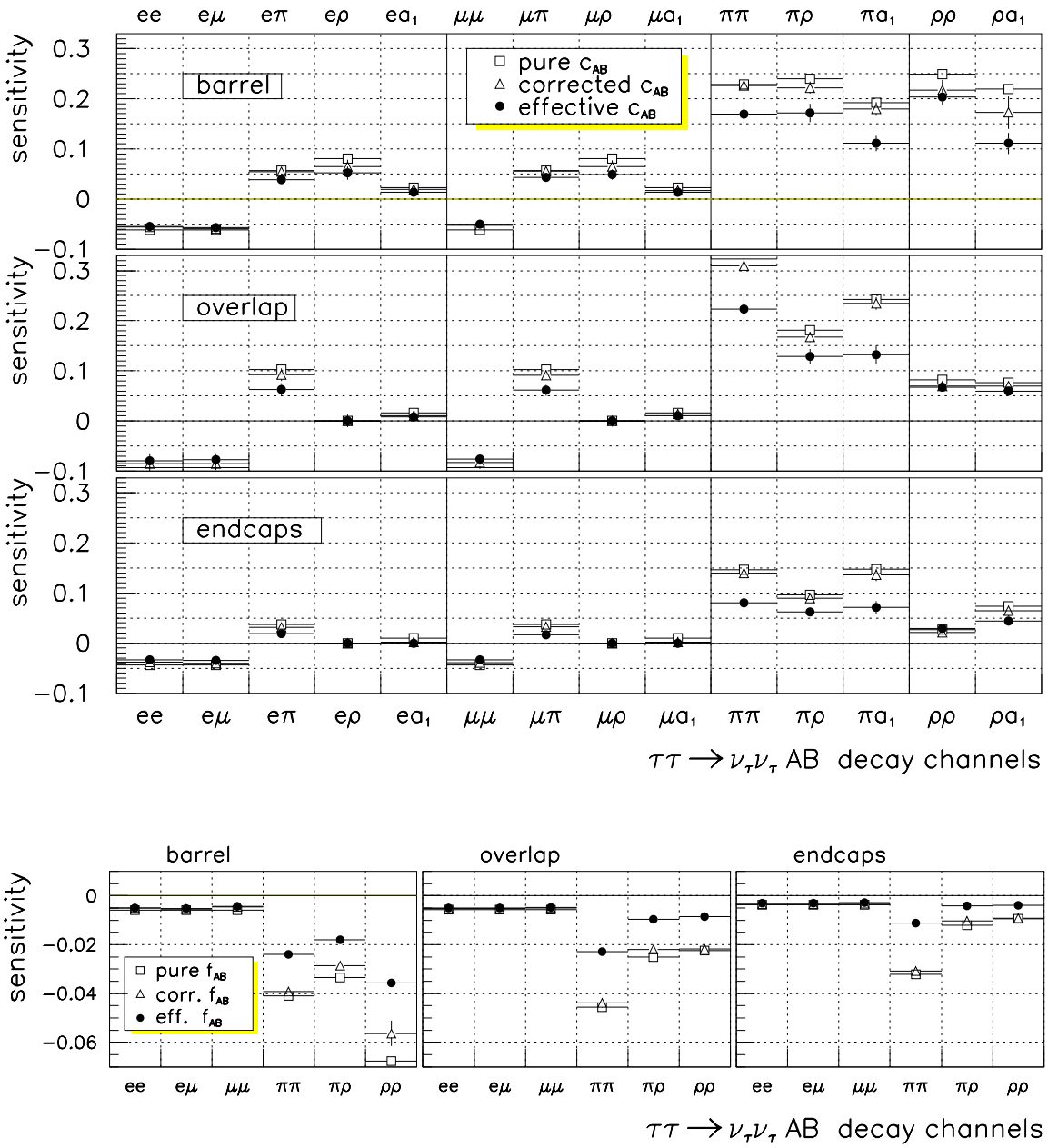

Figure 4: Sensitivities c_{AB} (top) and f_{AB} (bottom) of the $\tau^+\tau^-$ decay modes with respect to the three geometrical regions.

non-τ background is assumed to be insensitive to $\mathcal{CP}$-violation effects at the level of the uncertainty discussed here. For the τ-background, however, the influence on the sensitivities

[3] by P. Overmann, Phys. Inst. Dortmund

is taken into account for each individual channel. Since the $\mathcal{CP}$-odd observables are not optimized for the background decay modes the sensitivities of the τ decay channels are reduced proportional to their contamination by background sources. This is most evident for the $\tau^+\tau^- \to \pi^+\pi^-\,\nu\bar{\nu}$ events in the overlap region, where the degradation is about 30% due to the low purity. As mentioned in the previous section, the uncertainties in the quantitative determination of the background sources in the Monte Carlo simulation give rise to systematic errors on the sensitivities. The resulting systematic errors on the sensitivities are below 15% . Figure 4 shows the shifts of the sensitivities due to the mentioned systematic effects. The *pure* c_{AB} and f_{AB} are the original sensitivities calculated by numerical integration. The *corrected* sensitivities take into account the influence of the energy and momentum resolution of the detector. The *effective* sensitivities include background effects as well.

6 $\mathcal{CP}$-Symmetry of the Detector

In order to test the validity of our measurements, we have investigated the possibility that detector effects could fake CP-violation and hence the existence of a weak dipole moment of the τ. In polar coordinates, the following proportionalities hold

$$M_{\mathcal{CP}}^{\mathrm{Re}} \;\propto\; \sin(\phi^+ - \phi^-) \tag{16}$$

$$M_{\mathcal{CP}}^{\mathrm{Im}} \;\propto\; \cos(\theta^+ - \theta^-) \tag{17}$$

where ϕ is the azimuthal angle of a track in the $x-y$ plane and Θ its polar angle. These relations indicate how $\mathcal{CP}$-violation could be faked. If a systematic rotation of one side of the detector with respect to the opposite side exists, e.g. a systematic rotation of the two drift chamber flanges or the endcaps of the electromagnetic calorimeter, the distorted azimuth could lead to a non-zero mean value $\langle\sin(\phi^+ - \phi^-)\rangle$. Similarly, a systematic mismeasurement of one or both polar angles could give rise to a non-zero $\langle\cos(\theta^+ - \theta^-)\rangle$ and hence to a non-zero imaginary part of the dipole moment. In order to study this possibility we calculated the $\mathcal{CP}$-odd observables using events for which $\mathcal{CP}$-violation originating from the reaction itself can be excluded. The $\mathcal{CP}$-symmetry of the tracking chambers can be studied using $e^+e^- \to \mu^+\mu^-$ events. For about 38 700 of these events we typically find no deviation from zero within the statistical errors, for all observables considered and in the three geometrical regions of the detector. The precisions with which zero means could be reproduced were taken as upper limits on the systematic errors of the observables and are given in table 5 ($\Delta^{\mathrm{sys}}\langle\mathcal{O}^{\mathcal{T}\pm}\rangle$).

$\mathcal{CP}$-violation arising from experimental defects of the electromagnetic calorimeter or its alignment with the tracking chamber has also been studied; in the reconstruction of the ρ channel the electromagnetic calorimeter is used to measure the π^0. Artificially constructed $\tau^+\tau^- \to \pi^+\pi^0\,\pi^-\pi^0\,\nu_\tau\bar{\nu}_\tau$ events from different Z^0 decays are used (event mixing). These events are uncorrelated and can therefore not give rise to any $\mathcal{CP}$-violation by a physical interaction. The $\mathcal{CP}$ measurement applied to these mixed events show no deviation from zero. (See Table 5)

In summary, using intrinsically $\mathcal{CP}$-symmetric events all observables are consistent with zero. The errors on the mean values were always much smaller than the ones obtained

for the $\tau^+\tau^-$ events. We therefore conclude that the detector is CP-symmetric to a level of $\mathrm{Re}(d_\tau^{\mathrm{detector}}) < 4 \times 10^{-19}$ e·cm and $\mathrm{Im}(d_\tau^{\mathrm{detector}}) < 3 \times 10^{-18}$ e·cm, respectively, i.e. 19 and 14 times better than the limits reported here.

7 Results

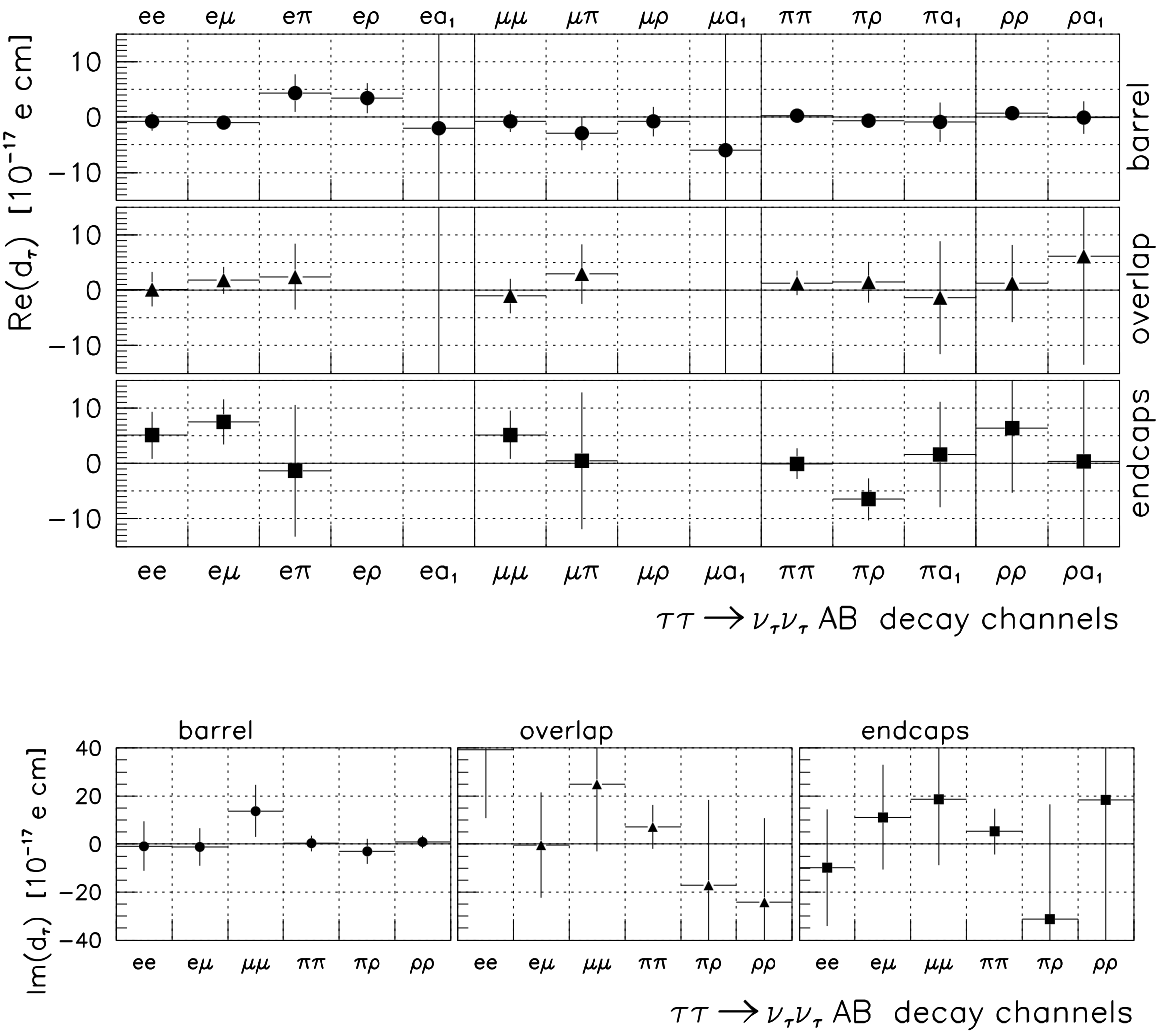

Figure 5: The real part (top) and the imaginary part (bottom) of the weak dipole moment in the considered $\tau^+\tau^-$ decay channels with respect to the three geometrical regions.

Using equation (3) the real and imaginary parts of the weak dipole moment of the τ can be determined by measuring the mean values of the CP-observables. Table 5 shows the effective sensitivities and both parts of the weak dipole moment obtained for the τ decay channels considered. The final values are obtained by calculating the weighted mean of the real and the imaginary parts of the weak dipole moment using Gaussian error propagation for the statistical and the non-correlated part of the systematic errors. The systematic errors of the sensitivities arising from detector resolution effects and $\Delta^{\mathrm{sys}}\langle \mathcal{O}^{T\pm} \rangle$ are treated

as correlated errors. The resulting errors are finally summed up quadratically with the non-correlated errors. The measured dipole moments are plotted in Figure 5. Figure 6 shows the distributions of the $\mathcal{CP}$ observables with respect to the three geometrical regions of the detector.

In total, we obtain for the real part of the weak dipole moment

$$\mathrm{Re}(d_\tau^w) \;=\; (\; -0.2 \;\pm\; 3.6_{\mathrm{stat}} \;\pm\; 1.4_{\mathrm{sys}} \;) \times 10^{-18}\; e \cdot \mathrm{cm}\;. \tag{18}$$

This value is consistent with zero, resulting in an upper limit of

$$\mathrm{Re}(d_\tau^w) \;<\; 7.9 \times 10^{-18}\; e \cdot \mathrm{cm} \tag{19}$$

at 95% confidence level.

For the imaginary part of the weak dipole moment we obtain

$$\mathrm{Im}(d_\tau^w) \;=\; (\; 0.95 \;\pm\; 1.55_{\mathrm{stat}} \;\pm\; 0.91_{\mathrm{sys}} \;) \times 10^{-17}\; e \cdot \mathrm{cm} \tag{20}$$

again consistent with zero, resulting in an upper limit of

$$\mathrm{Im}(d_\tau^w) \;<\; 4.5 \times 10^{-17}\; e \cdot \mathrm{cm} \tag{21}$$

at 95% confidence level. Since the sensitivities f_{AB} have not been calculated for all selected $\tau^+\tau^-$ decay modes (see Table 4), a factor of about 2.1 higher statistics was used in the determination of $\mathrm{Re}(d_\tau^w)$ compared to $\mathrm{Im}(d_\tau^W)$. Generally, the signal-to-noise ratio of the $\mathcal{CP}$-odd and $\mathcal{T}$-even observables is about 1.4 times lower compared to the $\mathcal{CP}$-odd and $\mathcal{T}$-odd observables. Therefore one expects a larger statistical error in the measurement of the imaginary part of the weak dipole moment. In both cases $\Delta_{\mathrm{sys}}/\Delta_{\mathrm{stat}}$ is below 59%.

8 Conclusions

Using 27 490 identified and reconstructed $\tau^+\tau^-$ events to measure $\mathcal{CP}$-odd and $\mathcal{T}$-odd observables sensitive to $\mathrm{Re}(d_\tau^w)$ and 12 834 $\tau^+\tau^-$ events to measure $\mathcal{CP}$-odd and $\mathcal{T}$-even observables sensitive to $\mathrm{Im}(d_\tau^w)$, no evidence for $\mathcal{CP}$-violation in the decay $\mathrm{Z}^0 \to \tau^+\tau^-$ has been found. The introduction of new, more sensitive $\mathcal{CP}$-odd observables resulted in a reduction of the statistical errors of up to a factor 2.4 compared to observables used in former analyses [15][16]. This analysis sets a precise upper limit on the real part of the $\mathcal{CP}$-violating weak dipole moment and, for the first time, on the imaginary part of the weak dipole moment:

$$\mathrm{Re}(d_\tau^w) \;<\; 7.9 \times 10^{-18}\; e \cdot \mathrm{cm} \;\; (95\%\ \mathrm{c.l.}) \tag{22}$$

$$\mathrm{Im}(d_\tau^w) \;<\; 4.5 \times 10^{-17}\; e \cdot \mathrm{cm} \;\; (95\%\ \mathrm{c.l.})\;. \tag{23}$$

As pointed out in the introduction, some models [17][18] predict that the electric and weak dipole moments of leptons scale with m^3_{lepton}. On this basis our limit compares favorably with those determined for the electron (23 times better) or the muon (3 times better) [19].

9 Acknowledgements

We gratefully acknowledge numerous helpful discussions with P. Overmann, W. Bernreuther and O. Nachtmann.
It is a pleasure to thank the SL Division for the efficient operation of the LEP accelerator, the precise information on the absolute energy, and their continuing close cooperation with our experimental group. In addition to the support staff at our own institutions we are pleased to acknowledge the
Department of Energy, USA,
National Science Foundation, USA,
Particle Physics and Astronomy Research Council, UK,
Natural Sciences and Engineering Research Council, Canada,
Israeli Ministry of Science,
Minerva Gesellschaft,
Japanese Ministry of Education, Science and Culture (the Monbusho) and a grant under the Monbusho International Science Research Program,
American Israeli Bi-national Science Foundation,
Direction des Sciences de la Matière du Commissariat à l'Energie Atomique, France,
Bundesministerium für Forschung und Technologie, FRG,
National Research Council of Canada, Canada,
A.P. Sloan Foundation and Junta Nacional de Investigação Científica e Tecnológica, Portugal.

decay channel	θ	$c^{\rm eff} \pm \Delta c^{\rm eff}$	$\langle \mathcal{O}^{\mathcal{T}^-} \rangle \pm \Delta^{\rm stat}\langle \mathcal{O}^{\mathcal{T}^-} \rangle \pm \Delta^{\rm sys}\langle \mathcal{O}^{\mathcal{T}^-} \rangle$	$\mathrm{Re}(d_\tau^w) \pm \Delta\mathrm{Re}(d_\tau^w)$	$\Delta^{\rm stat} d_\tau^w$	$\Delta^{\rm sys} d_\tau^w$
$e-e$	B	-0.0550 ± 0.0067	0.0018 ± 0.0043 ± 0.0002	-0.71 ± 1.70	1.69	0.12
	O	-0.0794 ± 0.0148	-0.0007 ± 0.0113 ± 0.0004	0.19 ± 3.09	3.09	0.11
	E	-0.0330 ± 0.0039	-0.0078 ± 0.0064 ± 0.0004	5.12 ± 4.26	4.20	0.66
$e-\mu$	B	-0.0572 ± 0.0056	0.0027 ± 0.0033 ± 0.0002	-1.02 ± 1.25	1.24	0.13
	O	-0.0774 ± 0.0125	-0.0064 ± 0.0088 ± 0.0004	1.79 ± 2.48	2.46	0.31
	E	-0.0340 ± 0.0070	-0.0118 ± 0.0059 ± 0.0004	7.53 ± 4.08	3.76	1.57
$e-\pi$	B	0.0387 ± 0.0047	0.0077 ± 0.0060 ± 0.0002	4.31 ± 3.41	3.36	0.53
	O	0.0626 ± 0.0132	0.0071 ± 0.0171 ± 0.0005	2.46 ± 5.95	5.92	0.54
	E	0.0194 ± 0.0036	-0.0012 ± 0.0106 ± 0.0003	-1.34 ± 11.86	11.84	0.42
$e-\rho$	B	0.0518 ± 0.0127	-0.0082 ± 0.0061 ± 0.0003	-3.43 ± 2.69	2.55	0.85
	O	-	-0.0039 ± 0.0181 ± 0.0005	-	-	-
	E	-	0.0091 ± 0.0115 ± 0.0004	-	-	-
$e-a_1$	B	0.0139 ± 0.0054	-0.0013 ± 0.0143 ± 0.0002	-2.02 ± 22.34	24.96	0.85
	O	0.0079 ± 0.0061	0.0176 ± 0.0384 ± 0.0005	48.34 ± 111.89	105.49	37.32
	E	-	-0.0082 ± 0.0194 ± 0.0003	-	-	-
$\mu-\mu$	B	-0.0499 ± 0.0054	0.0018 ± 0.0044 ± 0.0002	-0.78 ± 1.91	1.91	0.12
	O	-0.0756 ± 0.0115	0.0036 ± 0.0108 ± 0.0004	-1.03 ± 3.10	3.09	0.19
	E	-0.0329 ± 0.0050	-0.0078 ± 0.0065 ± 0.0004	5.14 ± 4.37	4.29	0.83
$\mu-\pi$	B	0.0435 ± 0.0049	-0.0059 ± 0.0060 ± 0.0002	-2.94 ± 3.01	2.99	0.34
	O	0.0616 ± 0.0107	0.0084 ± 0.0152 ± 0.0005	2.95 ± 5.38	5.45	0.54
	E	0.0172 ± 0.0034	0.0004 ± 0.0098 ± 0.0003	0.50 ± 12.37	12.33	0.39
$\mu-\rho$	B	0.0486 ± 0.0103	-0.0018 ± 0.0060 ± 0.0003	-0.80 ± 2.68	2.67	0.22
	O	-	0.0166 ± 0.0168 ± 0.0005	-	-	-
	E	-	0.0060 ± 0.0117 ± 0.0004	-	-	-
$\mu-a_1$	B	0.0138 ± 0.0054	-0.0038 ± 0.0153 ± 0.0002	-5.97 ± 24.17	18.64	2.35
	O	0.0104 ± 0.0064	-0.0148 ± 0.0263 ± 0.0005	-30.88 ± 58.08	54.87	19.03
	E	-	-0.0226 ± 0.0264 ± 0.0003	-	-	-
$\pi-\pi$	B	0.1699 ± 0.0231	0.0023 ± 0.0082 ± 0.0002	0.29 ± 1.04	0.92	0.47
	O	0.2238 ± 0.0327	0.0137 ± 0.0223 ± 0.0007	1.32 ± 2.17	2.16	0.20
	E	0.0801 ± 0.0136	-0.0001 ± 0.0104 ± 0.0002	-0.03 ± 2.81	2.81	0.05
$\pi-\rho$	B	0.1713 ± 0.0181	-0.0052 ± 0.0056 ± 0.0003	-0.66 ± 0.71	0.70	0.08
	O	0.1288 ± 0.0153	0.0086 ± 0.0222 ± 0.0008	1.45 ± 3.74	3.73	0.22
	E	0.0621 ± 0.0078	-0.0186 ± 0.0106 ± 0.0003	-6.49 ± 3.79	3.70	0.82
$\pi-a_1$	B	0.1110 ± 0.0155	-0.0047 ± 0.0169 ± 0.0002	-0.92 ± 3.53	3.53	0.14
	O	0.1321 ± 0.0185	-0.0084 ± 0.0620 ± 0.0007	-1.37 ± 10.19	10.19	0.22
	E	0.0714 ± 0.0121	0.0052 ± 0.0313 ± 0.0002	1.58 ± 9.51	9.51	0.27
$\rho-\rho$	B	0.2036 ± 0.0162	0.0065 ± 0.0074 ± 0.0004	0.69 ± 0.79	0.78	0.07
	O	0.0673 ± 0.0056	0.0039 ± 0.0216 ± 0.0009	1.25 ± 6.97	6.96	0.31
	E	0.0289 ± 0.0027	0.0085 ± 0.0155 ± 0.0004	6.38 ± 11.65	11.63	0.67
$\rho-a_1$	B	0.1110 ± 0.0211	-0.0003 ± 0.0151 ± 0.0003	-0.06 ± 2.95	2.95	0.06
	O	0.0591 ± 0.0065	0.0168 ± 0.0533 ± 0.0008	6.16 ± 19.58	19.57	0.74
	E	0.0438 ± 0.0062	0.0008 ± 0.0335 ± 0.0003	0.39 ± 16.59	16.58	0.16

decay channel	θ	$f^{\rm eff} \pm \Delta f^{\rm eff}$	$\langle \mathcal{O}^{\mathcal{T}^+} \rangle \pm \Delta^{\rm stat}\langle \mathcal{O}^{\mathcal{T}^+} \rangle \pm \Delta^{\rm sys}\langle \mathcal{O}^{\mathcal{T}^+} \rangle$	$\mathrm{Im}(d_\tau^w) \pm \Delta\mathrm{Im}(d_\tau^w)$	$\Delta^{\rm stat} d_\tau^w$	$\Delta^{\rm sys} d_\tau^w$
$e-e$	B	-0.0051 ± 0.0006	0.0002 ± 0.0022 ± 0 .0010	-0.85 ± 10.28	9.36	4.25
	O	-0.0049 ± 0.0006	-0.0089 ± 0.0059 ± 0 .0023	39.41 ± 28.45	26.12	11.27
	E	-0.0031 ± 0.0004	0.0014 ± 0.0033 ± 0 .0011	-9.80 ± 24.38	23.09	7.80
$e-\mu$	B	-0.0052 ± 0.0006	0.0003 ± 0.0016 ± 0 .0010	-1.25 ± 7.87	6.67	4.18
	O	-0.0050 ± 0.0008	0.0001 ± 0.0045 ± 0 .0023	-0.43 ± 21.93	19.53	9.98
	E	-0.0031 ± 0.0006	-0.0016 ± 0.0029 ± 0 .0011	11.2 ± 21.81	20.29	8.00
$\mu-\mu$	B	-0.0044 ± 0.0009	-0.0028 ± 0.0023 ± 0 .0010	13.81 ± 10.91	9.32	5.68
	O	-0.0048 ± 0.0010	-0.0055 ± 0.0056 ± 0 .0023	24.86 ± 27.85	32.31	11.61
	E	-0.0028 ± 0.0008	-0.0024 ± 0.0033 ± 0 .0011	18.6 ± 27.48	25.57	10.05
$\pi-\pi$	B	-0.0239 ± 0.0035	-0.0003 ± 0.0037 ± 0 .0002	0.27 ± 3.36	3.36	0.19
	O	-0.0228 ± 0.0045	-0.0076 ± 0.0095 ± 0 .0004	7.23 ± 9.16	9.04	1.48
	E	-0.0112 ± 0.0027	-0.0027 ± 0.0049 ± 0 .0002	5.23 ± 9.58	9.49	1.32
$\pi-\rho$	B	-0.0180 ± 0.0019	0.0025 ± 0.0044 ± 0 .0003	-3.01 ± 5.31	5.30	0.38
	O	-0.0097 ± 0.0013	0.0077 ± 0.0159 ± 0 .0005	-17.23 ± 35.66	35.57	2.56
	E	-0.0041 ± 0.0005	0.0059 ± 0.0090 ± 0 .0003	-31.22 ± 47.81	40.62	4.13
$\rho-\rho$	B	-0.0356 ± 0.0033	-0.0015 ± 0.0043 ± 0 .0004	0.91 ± 2.63	2.62	0.26
	O	-0.0085 ± 0.0005	0.0095 ± 0.0137 ± 0 .0006	-24.25 ± 35.04	34.97	2.09
	E	-0.0040 ± 0.0004	-0.0034 ± 0.0109 ± 0 .0004	18.44 ± 59.20	59.13	2.84

Table 5: Measurements of the real part and the imaginary part of the weak dipole moment for the respective τ decay channels in the three geometrical regions of the OPAL detector. In addition, the effective sensitivities are given, including detector and background corrections.

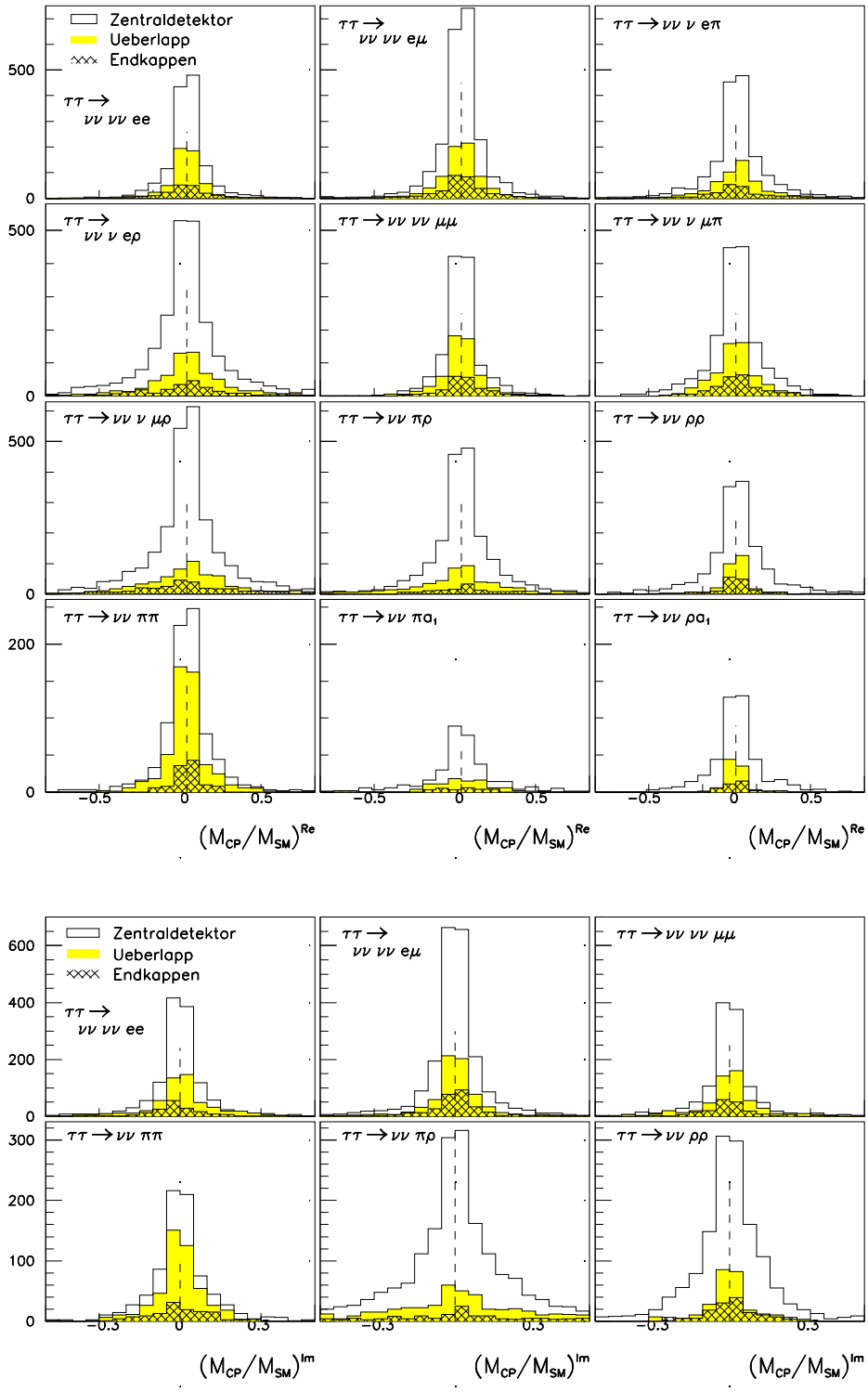

Figure 6: The measured $\mathcal{CP}$-odd, $\mathcal{T}$-odd (top) and $\mathcal{CP}$-odd, $\mathcal{T}$-even observables (bottom) from $Z^0 \to \tau^+\tau^-$ events of the 1991, 1992 and 1993 data.

A Application of a Likelihood Method to τ Decays

The classification of τ decays into the various τ decay modes is done using a maximum likelihood method. Good tracks and clusters are selected, the event is divided into two cones and the detector variables are calculated. The likelihood algorithm was applied to an individual cone using the following classification for 1-prong and 3-prong decay modes.
1-prong:

A $\tau \rightarrow e\nu_e\nu_\tau$

B $\tau \rightarrow \mu\nu_\mu\nu_\tau$

C $\tau \rightarrow \pi\nu_\tau$

D $\tau \rightarrow \rho\nu_\tau$

E $\tau \rightarrow a_1\nu_\tau$

3-prong:

A $\tau \rightarrow a_1\nu_\tau\,, a_1 \rightarrow 3\pi^\pm$

B $\tau \rightarrow K^*\nu_\tau$

C $\tau \rightarrow 3\pi^\pm \geq 1\pi^0\,\nu_\tau$

Due to a conversion of a (radiated) photon into two charged particles, the following 1-prong decay modes are reconstructed as 3-prong events

D $\tau \rightarrow e\nu_e\nu_\tau$

E $\tau \rightarrow \mu\nu_\mu\nu_\tau$

F $\tau \rightarrow \pi\nu_\tau$

G $\tau \rightarrow \rho\nu_\tau$

H $\tau \rightarrow a_1\nu_\tau\,, a_1 \rightarrow \pi^\pm 2\pi^0$.

From KORALZ 38/TAUOLA 15 Monte Carlo events for these decay channels, a reference distribution f_i^j for each variable i (see below) is generated.

The Detector Variables

The variables used to identify 1-prongs are: (See Figures 7 and 8)

EOVP Electromagnetic energy over charged momentum.

XELS Electromagnetic energy not assigned to the charged track.

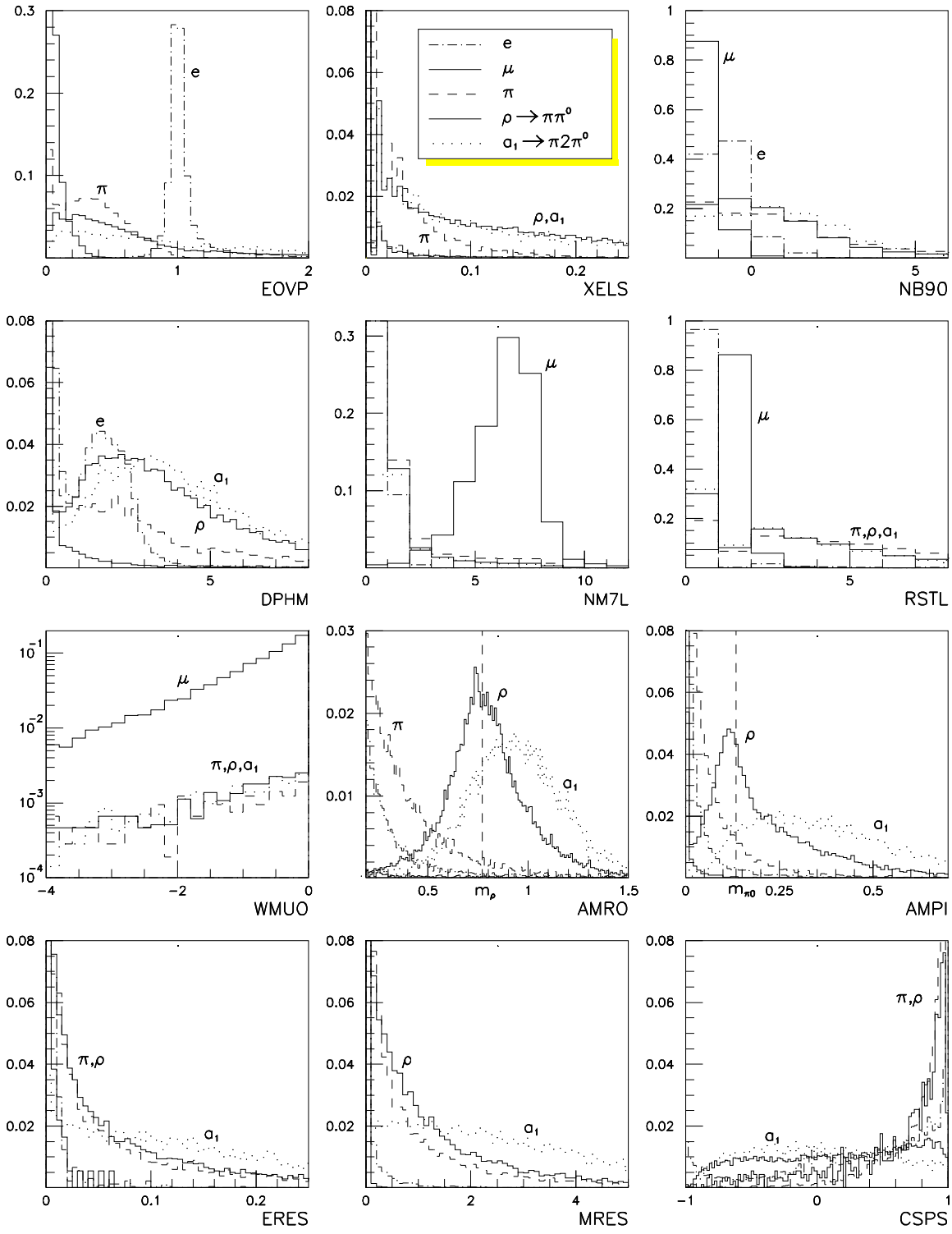

Figure 7: The normalized reference distributions of the 1-prong variables.

NB90 The minimum number of lead glass blocks containing at least 90 % of the cluster energy. The average value expected for electrons is subtracted. In the barrel this is simply a

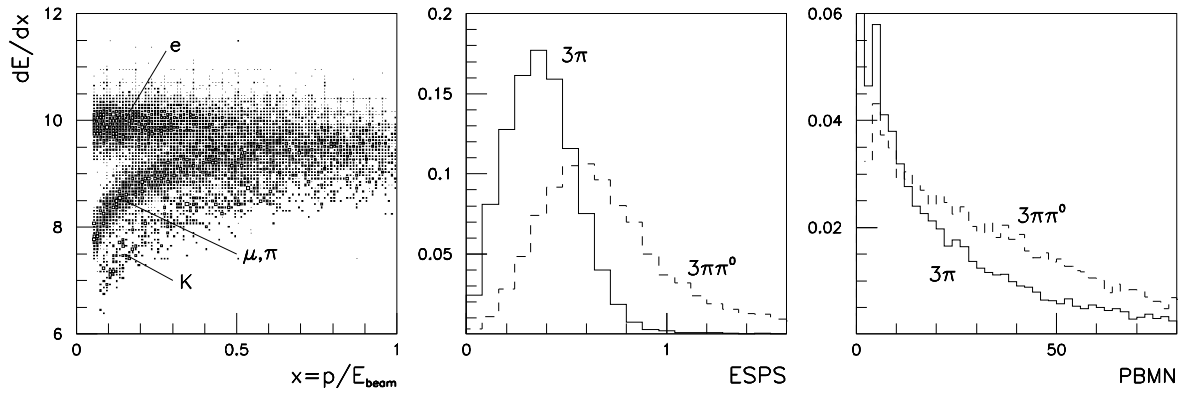

Figure 8: $\mathrm{d}E/\mathrm{d}x$ of the specific τ decay modes as a function of $x = p/E_{beam}$ (left) and the normalized reference distributions of the 3-prong variables.

shift by 2.19 blocks. But above 0.65 in $|\cos\theta|$ NB90 changes rapidly with $\cos\theta$ due to the material in front of the blocks and the non-projective geometry. This variation is taken into account by the subtraction.

DPHM The maximum angle between a presampler cluster and the charged track in the cone. (There is no coverage in the range $0.80 < \cos\theta < 0.82$.)

DEDX The deviation of the measured energy loss in CJ from the energy loss expected from the charged particle of each decay channel. The difference is measured in units of the error of the measurement.

NM7L The number of hits within the three last planes of the hadron calorimeter and the muon chambers.

RSTL The number of hits per layer in the hadron calorimeter.

WMUO Weight for the matching of the track segment in the muon chambers with the charged track.

The following 1-prong variables are based on a cluster algorithm developed in Tel Aviv for dedicated $\tau \to \rho\,\nu_\tau \to \pi\pi^0\,\nu_\tau$ analyses. It tries to decompose the supposed ρ energy pattern in the electromagnetic calorimeter into its three ingredient showers, using characteristic hadronic and electromagnetic shower patterns. Due to the non-projective geometry of the electromagnetic calorimeter in the endcaps, this cluster algorithm is only used in the barrel region. A detailed description is given in [20].

AMRO The invariant mass of the charged track with the reconstructed π^0, if any.

AMPI The invariant mass of the two reconstructed photons, if any.

MRES The residual mass in EB after subtraction of the ρ.

ERES The residual energy in EB after subtraction of the ρ.

CSPS The cosine of the angle of the pions in the ρ rest frame with respect to the ρ direction of flight.

The variables use to identify 3-prongs are:

PPIP The probability for each track to be an electron or a pion calculated from the dE/dx information is used to calculate the likelihood that all 3 tracks are pions compared to the likelihood they are 1 pion plus 2 electrons from a conversion.

VTXF The 3 tracks are fitted to a common vertex. The quality of the fit is used.

ESPS The ratio of electromagnetic energy over charged momentum, each summed over the cone.

PBMN The neutral presampler multiplicity (no track in a cone of 20 mrad around a PB cluster centroid).

The first two variables reduce the background from 1-prongs plus conversion. The last two variables distinguish between different 3–prong channels.

References

[1] F. Halzen, A.D. Martin, 'Quarks and Leptons', *John Wiley and Sons*, (1984)

[2] W. Bernreuther, U. Löw, J.P. Ma, O. Nachtmann, *Z. Phys. C - Particles and Fields* **43**, 117 (1989)

[3] P. Overmann, 'A new method to measure the tau polarization at the Z peak', *DO-TH* **93-24** (1993)

[4] W. Bernreuther, O. Nachtmann, P. Overmann, *Phys. Rev. D* **48**, 78, (1993)

[5] LEP-Collaborations and LEP Electroweak Working Group, *CERN-PPE*/**93-157**, (1993)

[6] J.H. Kühn, 'Tau kinematics from impact parameters', *TTP* **93-14**, (1993)

[7] Y.S. Tsai, *Phys. Rev.* **D4**, 2821 (1971)

[8] S. Jadach, J.H. Kühn and Z. Wąs, *Comput. Phys. Commun.* **64**, 275 (1991)

[9] M. Davier, L. Duflot, F. Le Diberder, A. Rougé *Phys. Lett.* **B306**, 411 (1993)

[10] OPAL Collaboration, P.D. Acton et al., *Phys. Lett.* **B288**, 373, (1992)

[11] J. Allison et al., *Nucl. Inst. and Meth.* **A317**, 47 (1992)

[12] J. Allison et al., *Comp. Phys. Comm.* **47**, 55 (1987)

[13] S. Jadach, B.F.L. Ward, Z. Wąs, *Comp. Phys. Comm.* **66**, 276 (1991)

[14] S. Jadach, J.H. Kühn, Z. Wąs, *Comp. Phys. Comm.* **64**, 275 (1991)

[15] OPAL Collaboration, P.D. Acton et al., *Phys. Lett.* **B281**, 405, (1992)

[16] ALEPH Collaboration, D. Buskulic et al., *Phys. Lett.* **B297**, 459, (1992)

[17] W. Bernreuther, O. Nachtmann, *Phys. Rev. Lett.* **63**, 2787, (1989)

[18] B. Krause, R. Decker, DPG-Frühjahrstagung Dortmund 1994, talk '$\mathcal{CP}$-verletzende Formfaktoren des Top-Quarks in Modellen mit erweitertem Higgssektor', Inst. f. theor. Teilchenph., Karlsruhe

[19] Particle Data Group, *Phys. Rev.* **D45**, Part 2, (1992)

[20] A. Beck, *OPAL*-**TN103**, (1992)